Tocopherol controls D1 amino acid oxidation by oxygen radicals in Photosystem II

Aditya Kumar[a], Ankush Prasad[a], Michaela Sedlářová[b], Ravindra Kale[c], Laurie K. Frankel[c], Larry Sallans[d], Terry M. Bricker[c,1], and Pavel Pospíšil[a,1]

[a]Department of Biophysics, Centre of the Region Haná for Biotechnological and Agricultural Research, Faculty of Science, Palacký University, 771 47 Olomouc, Czech Republic; [b]Department of Botany, Faculty of Science, Palacký University, 771 47 Olomouc, Czech Republic; [c]Department of Biological Sciences, Division of Biochemistry and Molecular Biology, Louisiana State University, Baton Rouge, LA 70803; and [d]The Rieveschl Laboratories for Mass Spectrometry, Department of Chemistry, University of Cincinnati, Cincinnati, OH 45221

Edited by Krishna K. Niyogi, University of California, Berkeley, CA, and approved December 15, 2020 (received for review September 11, 2020)

Photosystem II (PSII) is an intrinsic membrane protein complex that functions as a light-driven water:plastoquinone oxidoreductase in oxygenic photosynthesis. Electron transport in PSII is associated with formation of reactive oxygen species (ROS) responsible for oxidative modifications of PSII proteins. In this study, oxidative modifications of the D1 and D2 proteins by the superoxide anion ($O_2^{\bullet-}$) and the hydroxyl ($HO^{\bullet}$) radicals were studied in WT and a tocopherol cyclase (*vte1*) mutant, which is deficient in the lipid-soluble antioxidant α-tocopherol. In the absence of this antioxidant, high-resolution tandem mass spectrometry was used to identify oxidation of D1:^{130}E to hydroxyglutamic acid by $O_2^{\bullet-}$ at the $Pheo_{D1}$ site. Additionally, D1:^{246}Y was modified to either tyrosine hydroperoxide or dihydroxyphenylalanine by $O_2^{\bullet-}$ and $HO^{\bullet}$, respectively, in the vicinity of the nonheme iron. We propose that α-tocopherol is localized near $Pheo_{D1}$ and the nonheme iron, with its chromanol head exposed to the lipid–water interface. This helps to prevent oxidative modification of the amino acid's hydrogen that is bonded to $Pheo_{D1}$ and the nonheme iron (via bicarbonate), and thus protects electron transport in PSII from ROS damage.

reactive oxygen species | tocopherol | photosystem II | EPR | mass spectrometry

Photosystem II (PSII), a multiprotein complex present in the thylakoid membranes of oxygenic photosynthetic organisms, uses light to drive water oxidation and plastoquinone reduction (1–5). Under excess light, light-driven processes are associated with the formation of reactive oxygen species (ROS) by energy transfer and electron transport. In energy transfer, singlet oxygen ($^1O_2$) is formed by the energy transfer from triplet chlorophyll to molecular oxygen (6–8). In electron transport, ROS are formed by a concerted two-electron oxidation of water and a consecutive one-electron reduction of molecular oxygen (9). An incomplete oxidation of water by the Mn_4O_5Ca cluster may form hydrogen peroxide (H_2O_2) due to the uncontrolled delivery of water to the Mn_4O_5Ca cluster (10). The authors proposed that the uncontrolled delivery of water is caused by the removal of chloride from a water channel, as chloride depletion causes pronounced H_2O_2 formation (11, 12). The H_2O_2 is reduced to hydroxyl radical ($HO^{\bullet}$) by manganese, which partially dissociates from the metal cluster (10). A one-electron reduction of molecular oxygen by the redox-active cofactors pheophytin ($Pheo_{D1}^{\bullet-}$) and/or the plastosemiquinone at the Q_A site ($Q_A^{\bullet-}$) produces a superoxide anion radical ($O_2^{\bullet-}$). The $O_2^{\bullet-}$ either dismutes to free H_2O_2 or interacts with the nonheme iron to form bound peroxide. Both free and bound peroxide can be reduced to $HO^{\bullet}$ by free iron or the nonheme iron (13). Apart from PSII, Photosystem I (PSI) serves as a source of ROS in the thylakoid membrane. The PSI produces $O_2^{\bullet-}$, H_2O_2, $HO^{\bullet}$, and possibly $^1O_2$ (14); however, the sites of their production by PSI is the subject of significant debate. Plants have developed an intricate system of enzymatic (superoxide dismutase and catalase) and nonenzymatic (carotenoids, isoprenoid quinones, and tocochromanols) antioxidant mechanisms to prevent ROS damage within PSII (7, 15, 16).

The tocochromanols, α-tocopherol and plastochromanol-8, contain a hydrophilic chromanol head derived from tyrosine (shikimic acid pathway) and a hydrophobic polyprenyl side chain derived from the isoprenoid pathway (17). The chromanol head of α-tocopherol and plastochromanol-8 is responsible for their antioxidant function. When antioxidants are not able to effectively scavenge ROS, oxidative modification of several PSII proteins (D1, D2, CP43, CP47, and Lhcb3) occurs (18–21). Recent progress in identification of oxidized amino acid residues of the D1 and D2 proteins using high-resolution tandem mass spectrometry (MS) demonstrated that oxidized amino acid residues are localized primarily near the sites of ROS formation (10, 22–24). In an early study, Sharma et al. (25) showed a single oxidative modification on an unidentified amino acid residue of the D1 protein. More recently, we have identified a number of natively oxidized D1 and D2 residues in the vicinity of the manganese cluster and the redox active cofactors $Pheo_{D1}$ (D1:^{130}E, ^{133}L, and ^{135}F), Q_A (D2:^{238}P, ^{239}T, ^{242}E, and ^{247}M), and Q_B (D1:^{239}F, ^{241}Q, and ^{242}E) (22, 23). Oxidatively modified amino acids at the Q_A and Q_B sites are localized in the hydrophilic D-*de* loop region, which connects the transmembrane helices D and E of the D1 and D2 proteins. Congruent with this, the D-*de* loop in the D1 protein between amino acids 238 and 249 was proposed to be the region of the primary cleavage of D1 protein in vivo (19, 26).

Several studies showed the antioxidant activity of α-tocopherol in the protection of lipid oxidation by ROS; however, its antioxidant function in the protection of protein oxidation has not been fully explored in plants. Using inhibition of α-tocopherol

Significance

During oxygenic photosynthesis Photosystem II is damaged by reactive oxygen species (ROS). It is known that α-tocopherol protects the photosystem from a subset of this oxidative damage. The sites that were protected and the mechanisms leading to protein damage had not been determined. Herein, we identify the ROS responsible for damage on the reducing side of Photosystem II, the protein residues that are damaged by these ROS, and we propose a model localizing α-tocopherol within the photosystem yielding the observed protection.

Author contributions: A.K., L.K.F., L.S., T.M.B., and P.P. designed research; A.K., A.P., M.S., R.K., L.S., and T.M.B. performed research; A.K., T.M.B., and P.P. analyzed data; and A.K., L.K.F., T.M.B., and P.P. wrote the paper.

The authors declare no competing interest.

This article is a PNAS Direct Submission.

[1]To whom correspondence may be addressed. Email: btbric@lsu.edu or pavel.pospisil@upol.cz.

This article contains supporting information online at https://www.pnas.org/lookup/suppl/doi:10.1073/pnas.2019246118/-/DCSupplemental.

Published January 21, 2021.

synthesis in *Chlamydomonas reinhardtii*, immunoblot analysis of the D1 and D2 proteins showed loss of D1 and D2 proteins caused by $^1O_2$ (27). In our study, we investigated the oxidative modifications of the D1 and D2 proteins by $O_2^{\bullet-}$ and $HO^{\bullet}$ in Arabidopsis WT and the *vte1* mutant, which is deficient in α-tocopherol and plastochromanol-8. Herein, we provide evidence that α-tocopherol prevents oxidation of specific amino acid residues of the D1 protein on the PSII electron acceptor side. It should be noted that a protective role for plastochromanol-8 cannot be excluded, although the plastochromanol-8 content in leaves is much lower than α-tocopherol. We demonstrate that D1:^{130}E is oxidized by $O_2^{\bullet-}$ formed at the $Pheo_{D1}$ site and D1:^{246}Y is oxidized by $O_2^{\bullet-}$ and $HO^{\bullet}$ formed in the vicinity of the nonheme iron. It is suggested that the chromanol head group of α-tocopherol is exposed to the membrane surface. We propose that hydrogen bonding of D1:^{130}E to $Pheo_{D1}$ and of D1:^{246}Y to the nonheme iron via bicarbonate plays a crucial role in the regulation of electron transport from $Pheo_{D1}^{\bullet-}$ to Q_A and from $Q_A^{\bullet-}$ to Q_B.

Results

Formation of Superoxide Anion and Hydroxyl Radicals in Leaves and Thylakoid Membranes. To visualize formation of $O_2^{\bullet-}$ and $HO^{\bullet}$ in the high-intensity white light-exposed WT and *vte1 Arabidopsis*, the fluorescent probes dihydroxy ethidium (DHE) and 3′-p-(hydroxyphenyl) fluorescein (HPF) were used, respectively. Upon reaction with $O_2^{\bullet-}$ and $HO^{\bullet}$, DHE and HPF (low fluorescent) were oxidized to DHEox and HPFox (high fluorescent), respectively, and the DHEox and HPFox fluorescences detected by laser confocal scanning microscopy. As HPF is partially sensitive to $^1O_2$, possible oxidation of HPF to HPFox by $^1O_2$ cannot be ruled out (28). DHEox and HPFox fluorescences were measured in the high-intensity white light-exposed *Arabidopsis* leaves previously treated with DHE or HPF either in the dark or exposed to high-intensity red light to avoid photooxidation of the fluorescent probes. Figs. 1*A* and 2*A* show the Nomarski differential interference contrast (DIC) (Figs. 1*A* and 2*A*, *Left* column); DHEox or HPFox fluorescence (Figs. 1*A* and 2*A*, *Center* column), and chlorophyll (Chl) fluorescence (Figs. 1*A* and 2*A*, *Right* column) channels measured in *Arabidopsis* leaves. In the dark, low DHEox and HPFox fluorescences were observed in WT, whereas they were higher in *vte1* compared to WT. After exposure to high-intensity red light, the DHEox and HPFox fluorescences were enhanced in all samples. The DHEox and HPFox fluorescences in *vte1* were significantly higher compared to WT. The comparison of Nomarski DIC and DHEox or HPFox fluorescence channels revealed that $O_2^{\bullet-}$ and $HO^{\bullet}$ were formed predominantly in the chloroplasts. These results reveal that α-tocopherol is an effective scavenger of $O_2^{\bullet-}$ and $HO^{\bullet}$ in the leaf.

To confirm these results, we monitored the formation of $O_2^{\bullet-}$ and $HO^{\bullet}$ by electron paramagnetic resonance (EPR) using 5-tert-butoxycarbonyl-5-methyl-1-pyrroline-*N*-oxide (BMPO) and α-(4-pyridyl-1-oxide)-*N*-tert-butylnitrone (POBN)/ethanol spin traps, respectively, in the thylakoid membranes isolated from high-intensity white light-exposed WT and *vte1 Arabidopsis*. The BMPO spin trap interacts with $O_2^{\bullet-}$ and forms a BMPO-OOH adduct; similarly, POBN/ethanol interacts with $HO^{\bullet}$ and forms a POBN-CH(CH_3OH) adduct. No BMPO-OOH or POBN-CH(CH_3OH) adduct EPR signal was observed in the dark thylakoid membranes, whereas after exposure with high-intensity white light, BMPO-OOH and POBN-CH(CH_3OH) adduct EPR signals were observed (Figs. 1*B* and 2*B*), respectively. Comparison of the amplitude of the BMPO-OOH adduct EPR signals in WT and *vte1* (Fig. 1*B*) and POBN-CH(CH_3OH) adduct EPR signals in WT and *vte1* (Fig. 2*B*) observed at different time points in WT and *vte1* thylakoid membranes shows that $O_2^{\bullet-}$ and $HO^{\bullet}$ formation in *vte1* is higher compared to WT (Figs. 1*B* and 2*B*, *Bottom*), respectively. These EPR measurements in thylakoid membranes confirmed that α-tocopherol is an effective scavenger of $O_2^{\bullet-}$ and $HO^{\bullet}$ in *Arabidopsis*.

Formation of Protein Radicals in Leaves and Thylakoid Membranes. To visualize formation of protein radicals in the high-intensity white light-exposed WT and *vte1 Arabidopsis*, the 5,5-dimethyl-1-pyrroline *N*-oxide (DMPO) spin trap and an FITC-conjugated anti-DMPO antibody were used. The DMPO spin trap reacts with protein radicals and forms a protein radical-derived DMPO-nitrone adduct identified by anti-DMPO antibody. FITC fluorescence was detected by laser confocal-scanning microscopy in *Arabidopsis* leaves previously treated with DMPO and the FITC-conjugated anti-DMPO antibody either in the dark or exposed to high-intensity red light. Fig. 3 shows the combination of Nomarski DIC (Fig. 3*A*, *Left* column), fluorescence from FITC conjugated anti-DMPO antibody (Fig. 3*A*, *Center* column), and chlorophyll (Chl) fluorescence (Fig. 3*A*, *Right* column) channels measured in *Arabidopsis* leaves. In the dark, low FITC fluorescence was observed in WT, whereas it was higher in *vte1* compared to WT. After exposure with high-intensity red light, FITC fluorescence in *vte1* was significantly higher compared to WT, whereas there was no difference between dark and high intensity red light-exposed WT. The comparison of Nomarski DIC and FITC fluorescence channels revealed that protein radicals are formed predominantly in the chloroplasts; surprisingly, the *vte1* dark and red-light panel shows disruption of mesophyll cells and random scattering of chloroplast proteins. As Triton X-100 (0.001%) was added before exposure to high-intensity red light to assist in the infiltration of the spin trap and antibodies into the cells, it seems that Triton X-100 amplified disruption of mesophyll cells and scattering of proteins. These results reveal that α-tocopherol partially prevents the formation of protein radicals produced as a consequence of protein oxidation by $O_2^{\bullet-}$ and $HO^{\bullet}$ in *Arabidopsis*.

To detect carbon-centered radicals ($R^{\bullet}$), we monitored their formation by EPR using a POBN spin trap in the thylakoid membranes isolated from high intensity light-exposed WT and *vte1 Arabidopsis*. In the dark, no detectable POBN-R adduct EPR signal was observed in WT and *vte1* thylakoid membranes. The exposure of WT and *vte1* thylakoid membranes to high-intensity white light resulted in the generation of a POBN-R adduct EPR signal (Fig. 3*B*). Comparison of the amplitudes of the POBN-R adduct EPR signals in WT and *vte1* observed at different time points demonstrates that $R^{\bullet}$ formation in *vte1* is increased relative to WT (Fig. 3*B*, *Bottom*). These EPR measurements in thylakoid membranes confirmed that α-tocopherol is an effective scavenger of $O_2^{\bullet-}$ and $HO^{\bullet}$ which, if not scavenged, lead to higher formation of $R^{\bullet}$ in *vte1* thylakoid membranes after abstraction of hydrogen atoms from proteins.

Characterization of Protein Radicals and Protein Carbonyls in Thylakoid Membranes. To determine the oxidation of D1 and D2 proteins in WT and *vte1* thylakoid membranes, we detected the formation of protein radicals in the dark and high-intensity white light-exposed thylakoid membranes using SDS/PAGE followed by immunoblot analysis with anti-DMPO antibody, which was raised against the nitrone of DMPO (Fig. 4*A*, *Left*). DMPO nitrone adducts formed on different proteins were separated by SDS/PAGE, transferred to a nitrocellulose (NC) membrane and identified using anti-DMPO antibody. Proteins involved in the formation of protein radicals were visualized by applying a HRP-conjugated secondary antibody and using luminol as a chemiluminescent probe. The WT and *vte1* dark lanes show a similar profile of protein radical formation, with several weak protein bands at apparent molecular masses of 26, 32, 41, 47, and 68 kDa. After exposure with high-intensity white light, WT and *vte1* lanes show that the intensity of these protein bands increased and additional protein bands at apparent molecular masses of 58 and 18 kDa appeared.

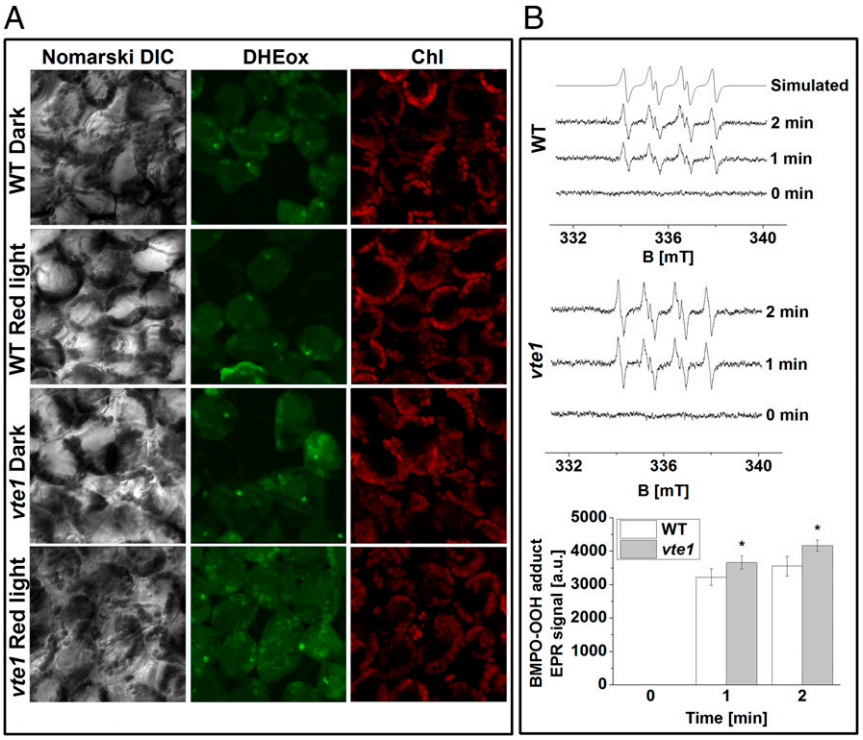

Fig. 1. (*A*) Superoxide anion radical imaging in *Arabidopsis* leaves monitored by laser confocal scanning microscopy. For $O_2^{\bullet-}$ imaging, 5 × 5-mm *Arabidopsis* leaf sections were incubated with 100 μM DHE either in the dark or exposed to high-intensity red light (1,000 μmol photons m^{-2} s^{-1}) for 30 min and DHEox fluorescence was detected. The panels (from *Left* to *Right*) show the Nomarski DIC, DHEox, and chlorophyll (Chl) fluorescence. Magnification, 1000×. (*B*) Superoxide anion radical detection in *Arabidopsis* thylakoid membranes monitored by EPR spectroscopy. Formation of $O_2^{\bullet-}$ was detected by EPR spectroscopy using a BMPO spin trap. To detect $O_2^{\bullet-}$, thylakoid membranes (250 μg of Chl mL^{-1}) were exposed to high-intensity white light (1,500 μmol photons m^{-2} s^{-1}) up to 2 min in the presence of 25 mM BMPO and 40 mM MES buffer (pH 6.5). The panels (*Top* to *Bottom*) illustrate the BMPO-OOH adduct EPR spectra in WT and *vte1,* and a time profile. The spectrum was simulated with hyperfine couplings of $a^N = 13.22$ and $a^H_\beta = 10.93$. To calculate significant differences, a Student's *t* test was used for comparison between high-intensity light-exposed WT and *vte1 Arabidopsis* thylakoid membranes. A significant difference between high-intensity light-exposed WT and *vte1* thylakoid membranes is indicated by the asterisk, * ($P < 0.05$). Two-way ANOVA was performed to show that at the 0.05 level, the population means of $O_2^{\bullet-}$ formation in high-intensity light-exposed WT and *vte1 Arabidopsis* are significantly different.

Oxidation of the D1 and D2 proteins was also explored by detecting the formation of protein carbonyls in dark- and high intensity light-exposed thylakoid membranes of WT and *vte1* by SDS/PAGE followed by immunoblot analysis with anti-DNP antibody (Fig. 4*A*, *Right*). WT dark- and high intensity light-exposed lanes show weak protein bands at apparent molecular masses of 26 and 47 kDa, whereas the *vte1* dark-exposed lane shows 26-, 34-, 47-, and 55-kDa protein bands. After exposure with high-intensity white light, *vte1* shows that the intensity of these protein bands increased with appearance of a broad indistinct band with an apparent molecular mass of >72 kDa. To confirm the loss of the D1 and D2 proteins by oxidation, immunoblot analysis was performed on stripped anti-DMPO and anti-DNP blots with anti-D1 and anti-D2 antibodies (Fig. 4*A*, *Lower*). Loss of D1 and D2 protein bands was observed in WT and *vte1* high intensity light-exposed samples. To determine if the chromanol head of α-tocopherol was exposed at the lipid–water interface, we used Trolox, a water-soluble analog of α-tocopherol, and performed SDS/PAGE followed by immunoblot analysis to detect the formation of protein radicals and protein carbonyls using anti-DMPO antibody (Fig. 4*B*, *Left*) and anti-DNP antibody (Fig. 4*B*, *Right*), respectively, in thylakoid membranes. The addition of the Trolox to the thylakoid membranes before high-intensity white light exposure decreased the intensity of the 26-, 32-, 41-, 47-, and 68-kDa bands in the anti-DMPO blot (Fig. 4*B*, *Left*) and 26-, 34-, 47-, 58-, and 68-kDa bands in the anti-DNP blot (Fig. 4*B*, *Right*). This result indicates that the water-soluble α-tocopherol analog can protect these proteins from modification. We also analyzed loss of the D1 and D2 proteins in the presence of Trolox on stripped anti-DMPO and anti-DNP blots with anti-D1 and anti-D2 antibodies (Fig. 4*B*, *Lower*). It was observed that Trolox prevents loss of the D1 and D2 proteins by oxidation under high-intensity light conditions. With respect to PSII in vivo, these results indicate that α-tocopherol protects the surface-exposed regions of the D1 and D2 proteins during high-intensity light stress.

Oxidation of Amino Acid Residues of D1 and D2 Proteins in Thylakoid Membranes. To identify the oxidative modifications on the amino acid residues of the D1 and D2 proteins, we performed MS analysis in samples prepared from the thylakoid membranes isolated from high-intensity light-exposed WT and *vte1 Arabidopsis* (Table 1). In WT, a number of amino acid residues were observed to be oxidatively modified, including the D1:^{317}W, ^{318}A, ^{329}E, ^{331}M, ^{332}H, and the D2:^{18}M, ^{246}M, ^{247}V, ^{328}W, ^{329}M, ^{341}F. Most of these residues (D1:^{317}W, ^{318}A, ^{329}E, ^{331}M, ^{332}H, and the D2:^{328}W, ^{329}M) are located in the C-terminal domain of the D1 and D2 proteins in the vicinity of the Mn_4O_5Ca cluster. Additional residues were modified in *vte1*, including D1:^{130}E, ^{131}W, and ^{132}E in the vicinity of $Pheo_{D1}$ (Figs. 5 and 6, black dotted circle) and D1:^{244}E, ^{246}Y, and ^{255}F in the vicinity of Q_A and the nonheme iron (Figs. 5 and 6, red dotted circle). These residues are all located on the stromal side of the membrane. Consequently, our results indicate that α-tocopherol prevents the oxidation of amino acid residues on the stromal side of PSII.

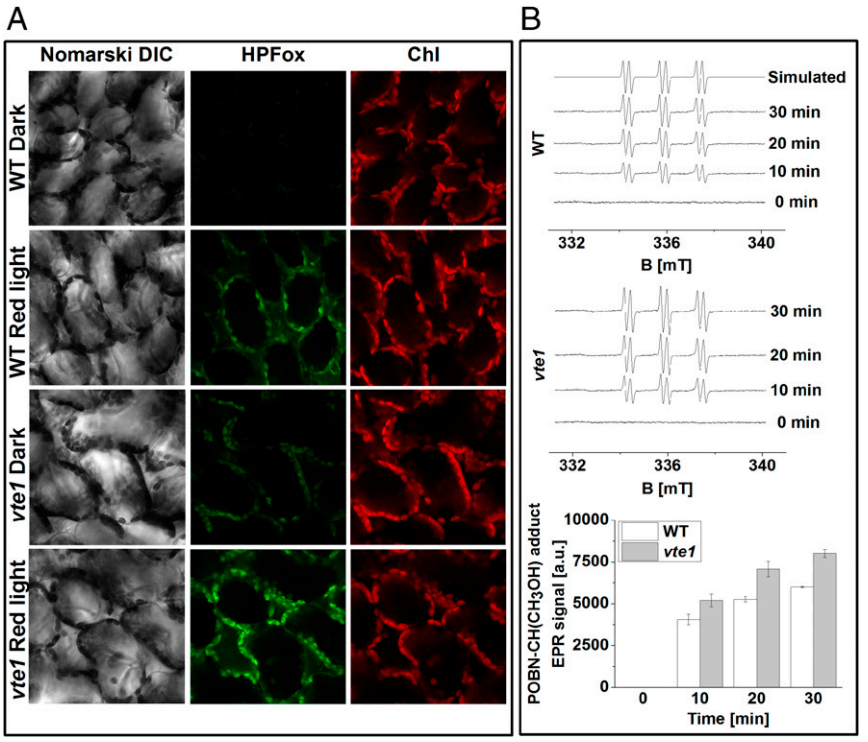

Fig. 2. (*A*) Hydroxyl radical imaging in *Arabidopsis* leaves monitored by laser confocal scanning microscopy. For $HO^{\bullet}$ imaging, 5 × 5-mm *Arabidopsis* leaf sections were incubated with 10 μM HPF either in the dark or exposed to high-intensity red light (1,000 μmol photons m^{-2} s^{-1}) for 30 min and HPFox fluorescence was detected. The panels (from *Left* to *Right*) show the Nomarski DIC, HPFox, and chlorophyll (Chl) fluorescence. Magnification, 1000×. (*B*) Hydroxyl radical detection in *Arabidopsis* thylakoid membranes monitored by EPR spectroscopy. Formation of $HO^{\bullet}$ was detected by EPR spectroscopy using a POBN spin trap in combination with ethanol. To detect $HO^{\bullet}$, thylakoid membranes (250 μg of Chl mL^{-1}) were exposed to high-intensity white light (1,500 μmol photons m^{-2} s^{-1}) for 30 min in the presence of 50 mM POBN, 170 mM ethanol, and 40 mM MES buffer (pH 6.5). The panels (*Top* to *Bottom*) illustrate the POBN-CH(CH_3OH) adduct EPR spectra in WT and *vte1*, and a time profile. The spectrum was simulated with hyperfine couplings of $a^N = 15.45$ and $a^H_\beta = 2.57$.

Discussion

Oxidative Modification of PSII Proteins by $O_2^{\bullet-}$ and $HO^{\bullet}$. Reduction of molecular oxygen by $Pheo_{D1}^{\bullet-}$ and $Q_A^{\bullet-}$ forms $O_2^{\bullet-}$ (Fig. 1), which may either be reduced to H_2O_2 or form a bound hydroperoxide by the interaction with the nonheme iron (9, 13, 29, 30). Subsequently, reduction of H_2O_2 by free metals or bound hydroperoxide by the nonheme iron results in the formation of $HO^{\bullet}$ (Fig. 2). The more pronounced production of $O_2^{\bullet-}$ in *Arabidopsis* leaves and thylakoid membranes of the α-tocopherol-lacking mutant *vte1* compared to WT (Fig. 1) reveals that α-tocopherol scavenges $O_2^{\bullet-}$. Similarly, higher $HO^{\bullet}$ formation in *Arabidopsis* leaves and thylakoid membranes of *vte1* compared to WT (Fig. 2) suggests that α-tocopherol either prevents the formation of $HO^{\bullet}$ by $O_2^{\bullet-}$ scavenging or directly scavenges $HO^{\bullet}$. When $O_2^{\bullet-}$ and $HO^{\bullet}$ are ineffectively scavenged by α-tocopherol, oxidative modification of proteins occurs in the vicinity of the sites of $O_2^{\bullet-}$ and $HO^{\bullet}$ formation. Imaging of protein radicals in *vte1* shows that α-tocopherol prevents formation of protein radicals in *Arabidopsis* leaves (Fig. 3*A*). Identification of protein radicals in *vte1* by standard blotting techniques using anti-D1 and anti-D2 antibodies shows that D1 and D2 proteins are predominantly oxidized (Fig. 4*A*). Protein oxidation is initiated by hydrogen abstraction from nearby amino acids which forms carbon-centered (alkyl) protein radicals. When molecular oxygen is not available, carbon-centered protein radicals can become cross-linked with other protein radicals to form protein aggregates. When molecular oxygen is available, oxygen-centered (peroxyl and alkoxyl) protein radicals are formed. Oxygen-centered protein radicals either propagate oxidation by other hydrogen abstraction from nearby amino acids or terminate oxidation by formation of the primary (hydroperoxides) and secondary (reactive carbonyl species and hydroxy-modified amino acid) products. When oxygen-centered protein radicals are formed on the protein backbone, protein fragmentation (cleavage of the D1 peptide bonds) can occur via β-scission of the protein alkoxyl radical, which forms a carbon-centered radical and carbonyl located either on the C-terminal or N-terminal fragments (Fig. 4*A*). The observation that water-soluble Trolox suppressed the formation of protein radicals reveals that oxidation of surface-exposed regions of the D1 and D2 proteins might be prevented by α-tocopherol during high-intensity light stress (Fig. 4*B*). Detailed analysis of oxidative modification of proteins by MS showed that D1:^{130}E, ^{131}W, and ^{132}E in the vicinity of $Pheo_{D1}$ and D1:^{244}E and ^{246}Y in the vicinity of nonheme iron are oxidized in the *vte1* mutant under high-intensity light stress (Table 1).

D1 Protein Oxidation by $HO_2^{\bullet}$ at the $Pheo_{D1}$ Site. Hydroperoxyl radical ($HO_2^{\bullet}$) formed by reduction of molecular oxygen by $Pheo_{D1}^{\bullet-}$ is proposed to oxidize D1:^{130}E, ^{131}W, and ^{132}E in the vicinity of $Pheo_{D1}$. General oxidation of D1:^{130}E in *vte1* suggests that glutamic acid is oxidized by $HO_2^{\bullet}$ to hydroxyglutamic acid (addition of one oxygen atom, +15.99 Da) (Table 1). It is generally accepted that $O_2^{\bullet-}$ (anionic form of superoxide) is rather unable to oxidize aliphatic amino acids, whereas $HO_2^{\bullet}$ (protonated form of superoxide) is considered to be more reactive toward aliphatic amino acids, with high capability to abstract hydrogen directly from nearby residues. It is well known that amino acids with a large number of aliphatic C–H bonds easily undergo hydrogen abstraction either from carbon at side chains or an α-carbon (carbon at backbone) (31). It is suggested that

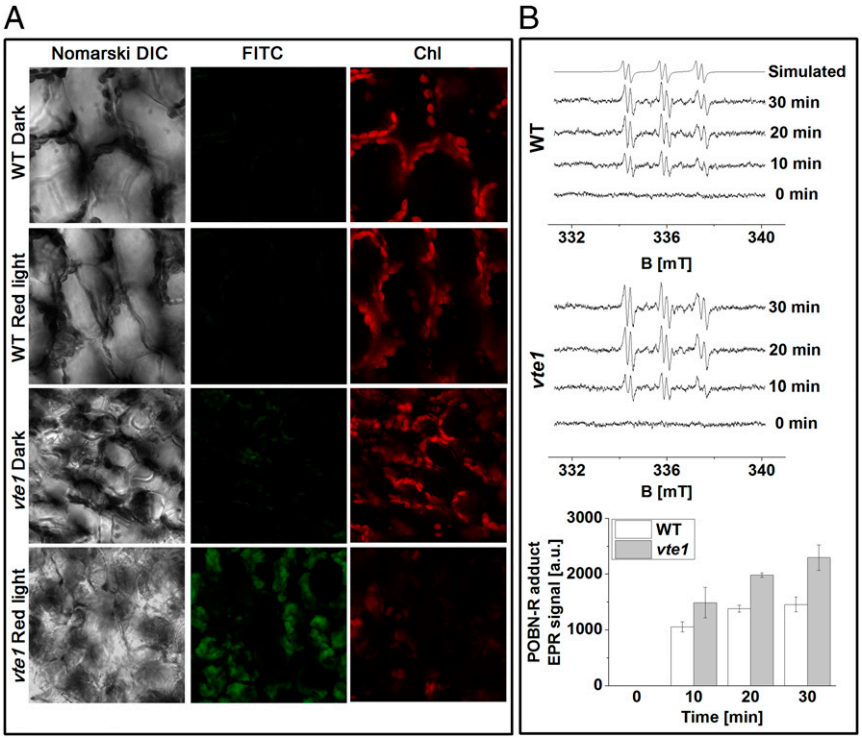

Fig. 3. (*A*) Protein radical imaging in *Arabidopsis* leaves monitored by laser confocal scanning microscopy. For protein radical imaging, 5 × 5 mm *Arabidopsis* leaf sections were incubated with 50 mM DMPO and 5 to 10 μg mL^{-1} FITC conjugated anti-DMPO antibody in the presence of 40 mM MES buffer (pH 6.5) and Triton X-100 (0.001%) either in the dark or exposed to high-intensity red light (1,000 μmol photons m^{-2} s^{-1}) for 30 min, and FITC fluorescence was detected. The panels (from *Left* to *Right*) show the Nomarski DIC, FITC, and chlorophyll (Chl) fluorescence. Magnification, 1000×. (*B*) Carbon-centered radical detection in *Arabidopsis* thylakoid membranes monitored by EPR spectroscopy. Formation of R• was detected by EPR spectroscopy using POBN spin trap. To detect R•, thylakoid membranes (250 μg of Chl mL^{-1}) were exposed to high intensity white light (1,500 μmol photons m^{-2} s^{-1}) for 30 min in the presence of 50 mM POBN and 40 mM MES buffer (pH 6.5). The panels (*Top* to *Bottom*) illustrate the POBN-R adduct EPR spectra in WT and *vte1*, and a time profile. The spectrum was simulated with hyperfine couplings of a^N = 15.40 and a^H_β = 2.38.

hydrogen abstraction from D1:^{130}E forms a carbon-centered protein radical formed at the C-3 or C-4 position on an aliphatic amino acid side chain of D1:^{130}E. The addition of molecular oxygen to C-3 or C-4 forms a protein peroxyl radical and subsequently a protein alkoxyl radical (*SI Appendix*, Fig. S2*A*). These protein peroxyl and alkoxyl radicals abstract another hydrogen from adjacent amino acid D1:^{131}W and initiate the propagation of protein oxidation. The hydrogen abstraction from C-2 of the indole ring of nearby D1:^{131}W by the alkoxyl radical formed at the C-3 or C-4 position on the aliphatic amino acid side chain of D1:^{130}E forms 3- or 4-hydroxyglutamic acid while a tryptophan radical is formed. Hydrogen abstraction from the adjacent amino acid D1:^{132}E by the tryptophan radical forms a carbon-centered protein radical formed at the C-3 or C-4 position on an aliphatic amino acid side chain of D1:^{132}E. Oxidation of D1:^{130}E amino acid residue in *vte1* at the distance of 3.6 Å from $Pheo_{D1}$ (Fig. 6*B*) suggests that $HO_2^•$ can diffuse from the site of its formation to the D1:^{130}E amino acid residue (Fig. 6*A*, black dotted arrows). The lack of repulsion of negative charge on the anionic form of superoxide and negative charge on the acidic side chains of glutamic acid allows $HO_2^•$ to diffuse to the C3 and C4 atoms of glutamic acid. Propagation of radical reactions on the D1 protein could continue from D1:^{130}E to nearby residues (D1:^{131}W and ^{132}E) (Fig. 6*A*, red dotted arrows), as the distances of D1:^{130}E from D1:^{131}W and D1:^{131}W from D1:^{132}E are each 1.3 Å.

D1 Protein Oxidation by HO• at the Nonheme Iron Site. Hydroxyl radical formed by reduction of bound hydroperoxide by the nonheme iron is assumed to oxidize D1:^{244}E and ^{246}Y in the vicinity of the nonheme iron. General oxidation of D1:^{246}Y in *vte1* suggests that D1:^{246}Y is oxidized by HO• to dihydroxyphenylalanine (DOPA) (addition of one oxygen atom, +16 Da) (Table 1). In this reaction, hydrogen abstraction from the hydroxyl group of the phenyl ring of D1:^{246}Y forms a tyrosyl radical, which is followed by delocalization of an unpaired electron from the oxygen to a carbon atom of the phenyl ring. The addition of another HO• to the phenyl ring forms DOPA (*SI Appendix*, Fig. S2*B*). As D1:^{246}Y is situated at the distance of 4.5 Å from the nonheme iron (Fig. 6*C*), HO• could possibly diffuse to D1:^{246}Y and react with D1:^{246}Y. Besides interacting with the nonheme iron, $O_2^{•-}$ interacts with the tyrosyl radical formed by oxidation of D1:^{246}Y by HO•. It is well established that $O_2^{•-}$ reacts with aromatic amino acids, particularly with the tyrosyl radical formed after hydrogen abstraction from the hydroxyl group of D1:^{246}Y phenyl ring (32). Double oxidation of the D1:^{246}Y amino acid residue in *vte1* suggests that the ^{246}Y amino acid residue is oxidized by $O_2^{•-}$ to tyrosine hydroperoxide (Tyr-OOH) (addition of two oxygen atoms, +32 Da) (Table 1) (33). It is proposed here that Tyr-OOH is formed by addition of $O_2^{•-}$ to the tyrosyl radical formed by hydrogen abstraction from D1:^{246}Y (*SI Appendix*, Fig. S2*B*). As D1:^{246}Y is situated at a distance of 10 Å from Q_A (Fig. 6*C*), it is suggested that $O_2^{•-}$ can diffuse from the site of its formation to the ^{246}Y amino acid residue (Fig. 6*A*, black dotted arrows). Apart from $O_2^{•-}$, Tyr-OOH might be formed by addition of $^1O_2$ to the phenyl ring (34). It is known that the diffusion distance of $^1O_2$ in thylakoid membranes is 55 Å (35). As D1:^{246}Y lies 30 Å from the site of putative $^1O_2$ formation by P_{680}, Tyr-OOH formation by addition of $^1O_2$ cannot be excluded. When the tyrosyl radical is not oxidized

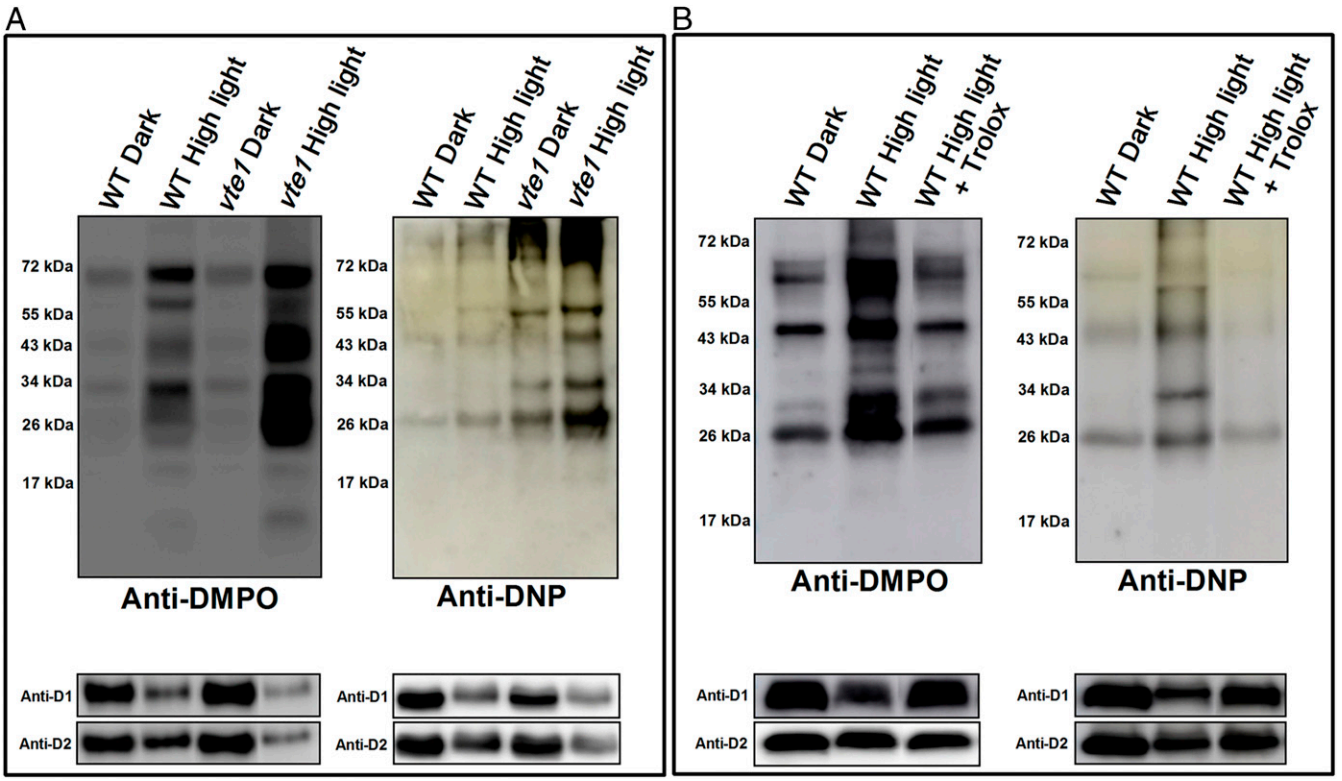

Fig. 4. Detection of protein radicals, and protein carbonyls and the D1 and D2 proteins in thylakoid membranes using immunoblotting. (*A*) Immunoblot showing protein radicals visualized with anti-DMPO and protein carbonyls visualized with anti-DNP. Loss of the D1 and D2 proteins in high-intensity light-exposed samples was detected using anti-D1 and anti-D2 antibodies on stripped anti-DMPO and anti-DNP blots. (*B*) Immunoblot of protein radicals visualized with anti-DMPO and protein carbonyls visualized with anti-DNP in the presence of 1 mM Trolox. Protection of the oxidation of the D1 and D2 proteins in high-intensity light-exposed samples by 1 mM Trolox was detected using anti-D1 and anti-D2 antibodies on stripped anti-DMPO and anti-DNP blots.

further by $O_2^{\bullet-}$ or $HO^{\bullet}$, it abstracts hydrogen from an adjacent D1:^{244}E and initiates propagation of protein oxidation (Fig. 6*A*, red dotted arrows). In this reaction, hydrogen abstraction by the tyrosyl radical forms an alkyl radical at the C-2 position on the aliphatic amino acid side chain of D1:^{244}E which delocalizes to C-3 or C-4 and subsequently forms protein peroxyl and alkoxyl radicals. The latter abstracts hydrogen from a nearby amino acid and forms 3- or 4-hydroxyglutamic acid (Table 1).

Two Sites of α-Tocopherol Localization in PSII. Based on the location of oxidized amino acid residues in *vte1*, we propose that α-tocopherol is located at least at two sites: One in the vicinity of $Pheo_{D1}$ nearby the D1:^{130}E (Fig. 7*A*) and another in the vicinity of the nonheme iron nearby the D1:^{246}Y amino acid residue (Fig. 7*B*) with its chromanol head exposed to the lipid–water interface. Location of the oxidized amino acid residues D1:^{246}Y and ^{130}E situated at about 13.5 Å from the lipid–water interface confirms that α-tocopherol antioxidant action takes place near the lipid–water interface, within the antioxidant activity zone proposed by Marquardt et al. (36) (*SI Appendix*, Fig. S3). Orientation and depth of the chromanol head in lipid bilayers can be diverse, as proposed by Fukuzawa et al. (37). The chromanol hydroxyl group can be located directly at the lipid–water interface region, slightly sunken into the membrane or deeply submerged into the bilayer. Orientation of the chromanol head slightly sunken into the membrane was supported by a small-angle X-ray diffraction study of brominated δ-tocopherol by Katsaras et al. (38), although the alternative orientation of the chromanol head's being parallel to the bilayer plane was also suggested (39).

Oxidation of D1:^{130}E and D1:^{246}Y May Modify Electron Transport. It is well established that the midpoint potential of the $Pheo_{D1}$/$Pheo_{D1}^{\bullet-}$ is affected by the strength of the hydrogen bond between $Pheo_{D1}$ and D1:^{130}E (40). It is proposed here that oxidation of D1:^{130}E to hydroxyglutamic acid disturbs hydrogen bonding and thus modifies electron transport from $Pheo_{D1}^{\bullet-}$ to Q_A. We proposed that α-tocopherol localized in the vicinity of the $Pheo_{D1}$ prevents hydroxyglutamic acid formation and thus protects electron transport from $Pheo_{D1}^{\bullet-}$ to Q_A at high-intensity light. Additionally, it has been recently demonstrated that hydrogen bonding from D1:^{246}Y and D2:^{244}Y to the bicarbonate ligand of the nonheme iron supports the stability of the semiquinones (41, 42). Using a quantum mechanical approach, Saito et al. (41) proposed that elongation of density at the hydroxy oxygen atom of D1:^{246}Y in the crystal structure from *Thermosynechococcus vulcanus* might be attributed to Tyr-OOH formed by X-ray radiation. An alternative hypothesis is that the putative Tyr-OOH is formed by light-induced oxidation of the tyrosyl residue prior to isolation of PSII. Saito et al. hypothesized that formation of Tyr-OOH at D1:^{246}Y possibly disrupts the hydrogen bonding from D1:^{246}Y to the bicarbonate ligand and disconnects the proton transfer path between bicarbonate and D1:^{215}H (41, 43). In addition, disruption of the hydrogen bonding from D1:^{246}Y to the bicarbonate ligand can shift the pK_a on bicarbonate and interrupt the bicarbonate-induced redox tuning responsible for the regulation of electron transfer to the plastoquinone pool (42). We suggest that α-tocopherol localized in the vicinity of the nonheme iron prevents Tyr-OOH formation at D1:^{246}Y and thus protects electron transport from $Q_A^{\bullet-}$ to Q_B at high-intensity light.

Table 1. Oxidative modifications of the PS II D1 and D2 proteins in WT and *vte1*

Protein	WT	*vte1*
D1		^{130}E + go*
		^{131}W+go
		^{132}E+go
		^{244}E+go†,de
		^{246}Y + go,do
		^{255}F+go
	^{317}W+go,kyn	^{317}W+go,kyn
	^{318}A+go	^{318}A+go
	^{329}E+go	^{329}E+go
	^{331}M+go	^{331}M+go
	^{332}H+go	^{332}H+go
D2	^{18}M+do,go	^{18}M+go
	^{246}M+go	^{246}M+go
	^{247}V+go	^{247}V+go
	^{328}W+go,do	^{328}W+go,do
	^{329}M+go,do	^{329}M+go,do
	^{341}F+go	^{341}F+go

It should be noted that we searched for 12 different amino acid modifications; these 4 were the only ones observed.

*Oxidative modifications key: de, Glu/Asp decarboxylation, −30.01 Da; do, double oxidation, +31.99 Da; go, general oxidation, +15.99 Da; kyn, kynurenine, +3.99 Da.

†In some instances, particular peptides were observed that bore different oxidative modifications at a single amino acid residue; these are separated by commas.

Materials and Methods

Plant Material and Thylakoid Membrane Isolation. *Arabidopsis thaliana* used in this study were: WT (Columbia-0); *vte1*, the tocopherol-lacking mutant (carrying a splice-site mutation in the candidate gene for tocopherol cyclase At4g32770 and devoid of *vte1* mRNA) (44). Seeds were obtained from the Nottingham *Arabidopsis* Stock Center, United Kingdom. A Phytotron, Fytoscope FS-WI-HY (Photon Systems Instruments) was used to grow the plants in a regulated environment (light intensity of 100 μmol photons m^{-2} s^{-1}, photoperiod of 8-h light/16-h dark and temperature of 22/20 °C (unless specified otherwise) with 60% relative air humidity. An AlgaeTron AG 230 (Photon Systems Instruments) was used to regulate the treatment with high-intensity white light (1,500 μmol photons m^{-2} s^{-1}) and cool air temperature (8 °C for 13 h) of *Arabidopsis* plants which were 5 to 6 wk of age. *Arabidopsis* plants had been exposed to the high-intensity white light were then used to prepare thylakoid membranes according to the protocol of Casazza et al. (45). These thylakoids were stored at −80 °C in the dark until use.

Determination of α-Tocopherol by HPLC. The α-tocopherol was detected by reverse-phase high-performance liquid chromatography (HPLC) using the Alliance e 2695 HPLC System (Waters) equipped with a 2475 Fluorescence (FLR) detector (λ_{ex} = 290 nm, λ_{em} = 330 nm) (*SI Appendix*, Fig. S1). The α-tocopherol extracted in methanol were injected onto a LiChrospher 100 RP-18 (5 μm) LiChroCART 250-4 (Merck) with isocratic analysis (0.8 mL min^{-1} at 25 °C) performed using a mobile phase [methanol: hexane, 17:1 (vol/vol) ratio].

Imaging of Superoxide Anion and Hydroxyl Radicals by Confocal Laser-Scanning Microscopy. Imaging of $O_2^{\bullet-}$ and $HO^{\bullet}$ is based on their reaction with fluorescent probes, DHE and HPF purchased from Sigma Aldrich and Thermo Fisher Scientific, respectively, and was performed using confocal laser-scanning microscopy. To minimize any potential artifactual fluorescence due to photooxidation of the fluorescent probes DHE and HPF caused by white light, the entire procedure was performed under either dark conditions or red light. The fluorescent probes DHE (100 μM) and HPF (10 μM) were infiltrated into 5 × 5-mm leaf pieces and incubated for 30 min either in the dark or exposed to high intensity red light (1,000 μmol photons m^{-2} s^{-1}), using an LED source with a CL6000 LED Zeiss light guide (Carl Zeiss Microscopy). A long-pass edge interference filter (λ > 600 nm) (Andover Corporation) was used during exposure. Subsequently, leaf pieces were shifted into fresh 40 mM MES buffer (pH 6.5) on a glass slide and visualized by confocal laser-scanning microscopy (Fluor view 1,000 unit attached to an IX80 microscope; Olympus Czech Group). The excitation of DHE and HPF was achieved using a 488-nm line of an argon laser and the emission was detected by a 505/605-nm

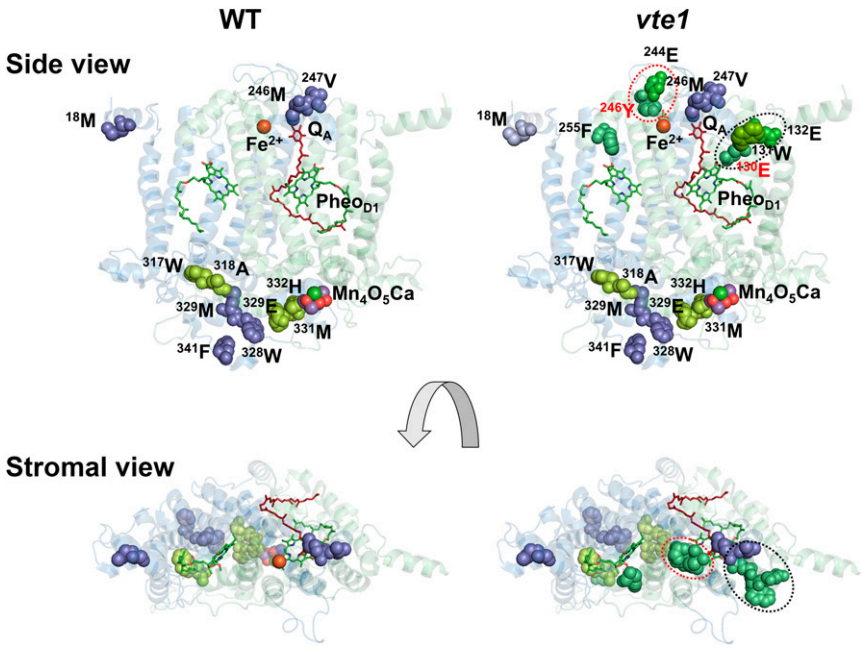

Fig. 5. Visualization of oxidative modifications of the D1 (green) and D2 (blue) proteins. Appearance of oxidative modifications of the D1 and D2 proteins presented as side and stromal views of WT and *vte1*. The D1 and D2 proteins are shown in green and blue, respectively. Oxidized amino acid residues are shown as spheres. Amino acid residues of the D1 protein modified only in *vte1* are shown in progressively darker shades of green outlined by dashed ovals. The Mn_4O_5Ca cluster (Mn, green; O, red; and Ca, blue) and the nonheme iron (brown) are shown as spheres. Pheo$_{D1}$ and Q_A are rendered as pale green and dark red sticks, respectively. All oxidized residues identified in Table 1 are illustrated in this figure. The protein structure used for visualization is from spinach PSII PDB ID: 3JCU (57).

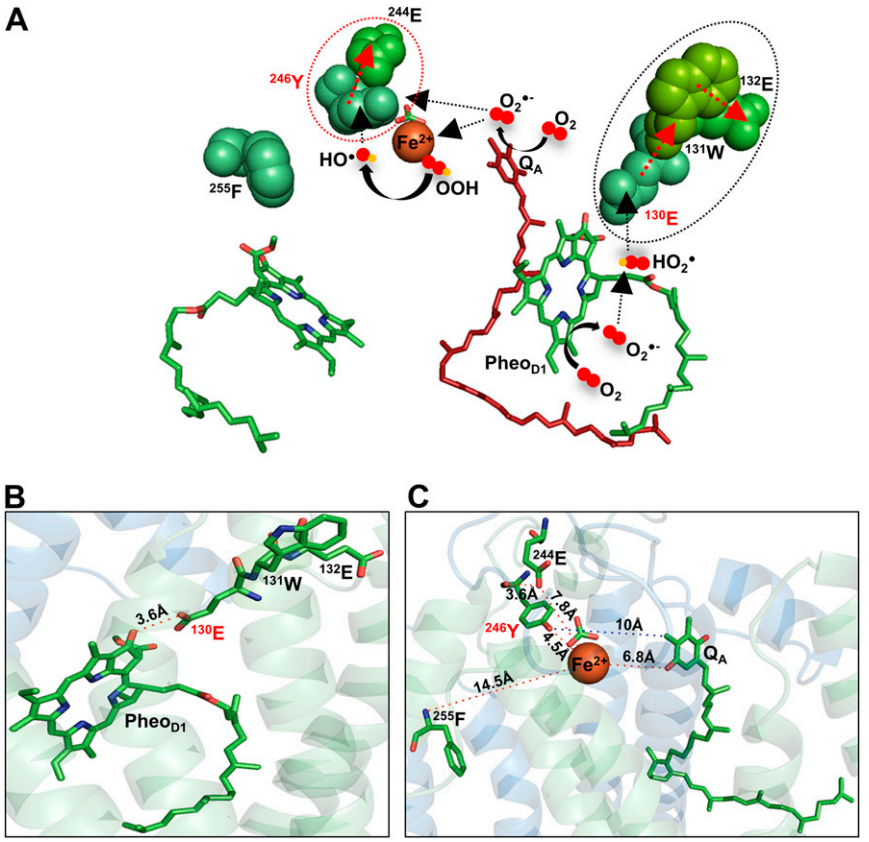

Fig. 6. (*A*) Amino acid oxidation in the vicinity of $Pheo_{D1}$ and nonheme iron in the absence of α-tocopherol. Both $Pheo_{D1}^{\bullet-}$ and $Q_A^{\bullet-}$ reduce molecular oxygen to $O_2^{\bullet-}$. Interaction of $O_2^{\bullet-}$ with nonheme iron forms bound peroxide, which is reduced to $HO^{\bullet}$. At the $Pheo_{D1}$ site, $HO_2^{\bullet}$ formed by protonation of $O_2^{\bullet-}$ can diffuse and oxidatively modify D1:^{130}E. The oxidative reaction continues to nearby residues D1:^{131}W and ^{132}E. At the nonheme iron, $HO^{\bullet}$ and $O_2^{\bullet-}$ can diffuse and oxidatively modify D1:^{246}Y, which continues to nearby residues D1:^{244}E. Darker shades of green represent subsequent oxidation events. Red dotted arrows show possible propagation pathways of radical reactions from residues in the vicinity of $Pheo_{D1}$ and nonheme iron to residues that are more distant from these sites. (*B*) Distance between D1:^{130}E and $Pheo_{D1}$. (*C*) Distances between amino acids, Q_A and nonheme iron. The protein structure used here for visualization is from spinach PSII PDB ID: 3JCU (57).

filter for DHE and 505/525-nm filter for HPF. The cell morphology was visualized using a 405-nm diode laser for excitation by a transmitted light detection module and DIC filters (46, 47).

Imaging of Protein Radicals by Confocal Laser-Scanning Microscopy. Imaging of protein radicals in leaves is based on the interaction of protein-centered radicals with the DMPO (Dojindo Molecular Technologies) spin trap, which forms a protein radical-derived DMPO nitrone adduct. Protein radical derived DMPO nitrone adducts were recognized by FITC-conjugated mouse monoclonal anti-DMPO antibody (Abcam) and visualized by confocal laser-scanning microscopy. Imaging of protein radicals in leaves was performed according to the protocol described in Kumar et al. (48). In brief, *Arabidopsis* leaves were placed on a glass slide with 40 mM MES buffer (pH 6.5) and cut into 5-mm^2 square leaf pieces, these leaf pieces were incubated under high-intensity red light (1,000 μmol photons m^{-2} s^{-1}) with 50 mM DMPO, 5 to 10 μg mL^{-1} FITC conjugated anti-DMPO antibody, and 40 mM MES buffer (pH 6.5) for 30 min at 25 °C. Triton X-100 (0.001%) was used during incubation to facilitate the infiltration of the spin trap and antibody into the cells. The FITC conjugated to mouse monoclonal anti-DMPO antibody was excited by a 488-nm line of an argon laser and the fluorescence signal was detected by a 505/550-nm emission filter to visualized protein radicals by confocal laser-scanning microscopy.

Detection of Superoxide Anion, Hydroxyl, and Carbon-Centered Radicals by EPR Spectroscopy. Formation of $O_2^{\bullet-}$ and $HO^{\bullet}$ was detected by EPR spectroscopy using BMPO (Dojindo Molecular Technologies) and POBN/ethanol (Enzo Life Sciences) spin traps, respectively. To detect $O_2^{\bullet-}$ and $HO^{\bullet}$, thylakoid membranes (250 μg of Chl mL^{-1}) were exposed to high-intensity white light (1500 μmol photons m^{-2} s^{-1}) for 2 min and 30 min in the presence of 50 mM BMPO, 40 mM MES buffer (pH 6.5), or 50 mM POBN, 170 mM ethanol and 40 mM MES buffer (pH 6.5), respectively. Formation of $R^{\bullet}$ was detected by EPR spectroscopy using a POBN spin trap. To detect $R^{\bullet}$, thylakoid membranes (250 μg of Chl mL^{-1}) were exposed to high-intensity white light (1,500 μmol photons m^{-2} s^{-1}) for 30 min in the presence of 50 mM POBN, 40 mM MES buffer (pH 6.5). EPR spectra were recorded at room temperature using an EPR spectrometer (MiniScope MS400, Magnettech). Intensity of the EPR signals was measured by the height of the second peak (for $O_2^{\bullet-}$) and the first peak of the central doublet (for $HO^{\bullet}$ and $R^{\bullet}$) of the first derivative of the EPR absorption spectrum. EPR conditions were as follows: Microwave power, 10 mW; modulation amplitude, 1 G; modulation frequency, 100 kHz; sweep width, 100 G; scan rate, 1.62 G s^{-1}. Simulation of EPR spectra was done using Winsim software (v0.96) (49).

Detection of Protein Radicals by Immuno-Spin Trapping. Detection of protein radicals in thylakoid membranes was performed according to the protocol described in Kumar et al. (48). In brief, thylakoid membranes (5 μg Chl) were incubated in the dark or exposed to high-intensity white light (1,500 μmol photons m^{-2} s^{-1}) with 50 mM DMPO for 30 min at 25 °C. Dithiothreitol (DTT) protein extraction buffer was used for the extraction of total protein from thylakoid membranes. Subsequent heating at 70 °C for 15 min and centrifugation at 16,000 × *g* for 5 min at room temperature was performed. Detection of protein carbonyls in thylakoid membranes was performed by incubating thylakoid membranes (5 μg Chl) under the dark or high-intensity white light (1,500 μmol photons m^{-2} s^{-1}) for 30 min at 25 °C. Afterward derivatization was performed by incubating the sample (5 μL) in a solution containing 12% aqueous sodium dodecyl sulfate (SDS; 5 μL) and 10 mM 2,4-dinitrophenylhydrazine (DNPH) dissolved in 2 M HCl (10 μL). The derivatization reaction was stopped after 15 min by adding neutralization buffer (7.5 μL) composed of 2 M Tris base and 30% glycerol (Sigma Aldrich). Protein samples were then separated by electrophoresis following the protocol

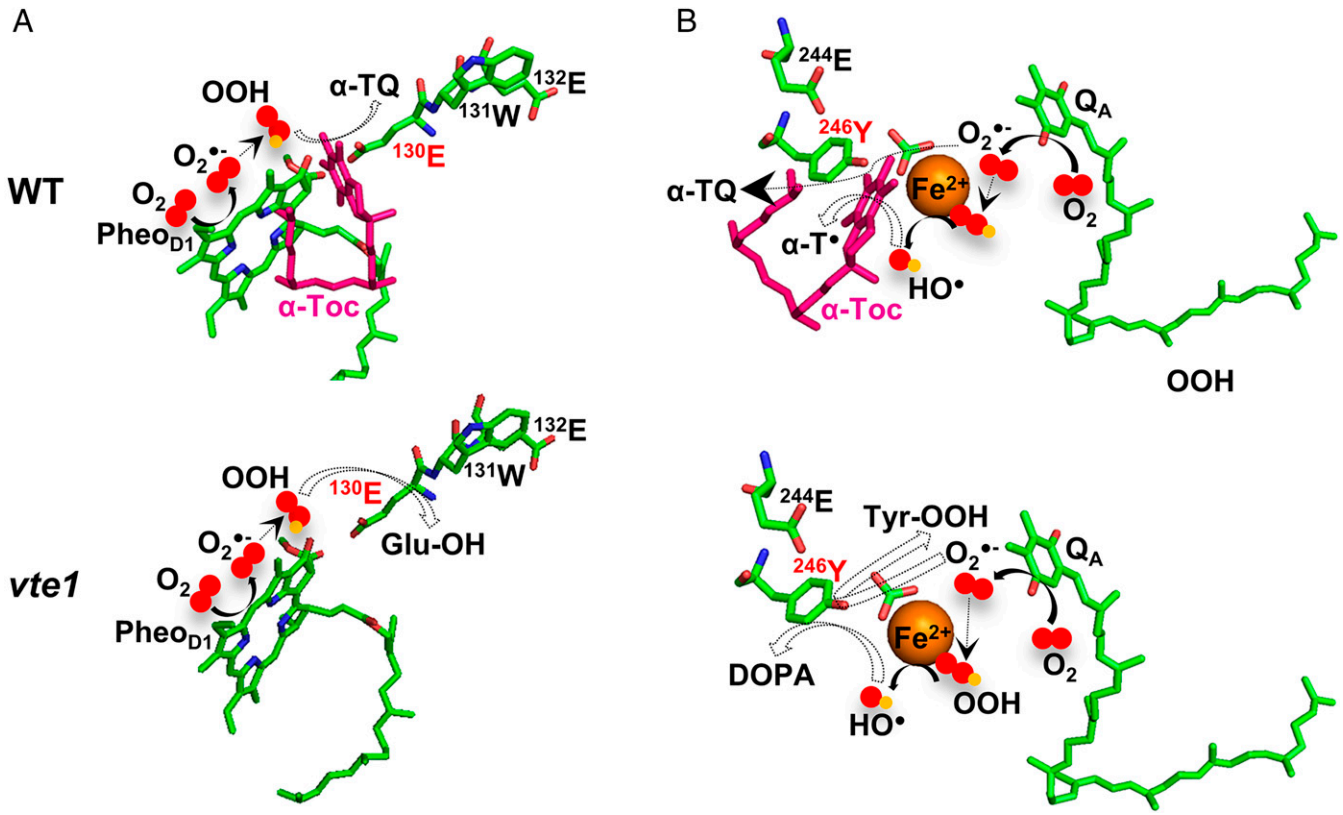

Fig. 7. Proposed mechanism for the scavenging of superoxide anion and hydroxyl radicals by α-tocopherol in PSII. (*A*). In WT, α-tocopherol is localized between $Pheo_{D1}$ and D1:^{130}E and prevents the oxidation of D1:^{130}E by scavenging $O_2^{\bullet-}$/$HO_2^{\bullet}$. Interaction of $O_2^{\bullet-}$ with α-tocopherol forms α-TQ. In *vte1*, absence of α-tocopherol leads to oxidation of D1: ^{130}E by $O_2^{\bullet-}$/$HO_2^{\bullet}$. (*B*) In WT, α-tocopherol is localized between the nonheme iron and D1:^{246}Y and hinders the oxidation of D1:^{246}Y either by preventing the formation of $HO^{\bullet}$, or by scavenging $O_2^{\bullet-}$ or $HO^{\bullet}$ directly. Interaction of $HO^{\bullet}$ and $O_2^{\bullet-}$ with α-tocopherol forms an α-tocopheroxyl radical (α-T$^{\bullet}$) and an α-tocopherol quinone (α-TQ), respectively. In *vte1*, absence of α-tocopherol leads to oxidation of D1:^{246}Y by $HO^{\bullet}$ or $O_2^{\bullet-}$ to DOPA and Tyr-OOH, respectively. The protein structure used here for visualization is from spinach PSII PDB ID: 3JCU (57).

described by Schägger (50). After electrophoresis, separated proteins were blotted to the NC membrane by using a semidry blotter (Trans-Blot SD, semidry transfer cell; Bio-Rad). The NC membranes were then incubated overnight at 4 °C in 5% BSA blocking solution prepared in phosphate-buffered saline tween (PBST; pH 7.4). The NC membranes were then probed with rabbit polyclonal anti-DMPO antibody (Abcam) and rabbit polyclonal anti-DNP antibody (Molecular Probes Europe BV). The NC membranes were then probed with HRP-conjugated anti-rabbit secondary antibody. Upon addition of the luminol as a chemiluminescent probe, the chemiluminescence signal was captured with an Amersham Imager 600 (GE Health Care Europe). Identification of D1 and D2 proteins was performed using anti-D1 and anti-D2 antibodies (Agrisera), respectively, on stripped blots. Stripping of anti-DMPO and anti-DNP antibody from the NC membranes was achieved by treating the NC membranes with 200 mM glycine-HCl (pH 2.2), 0.1% SDS, and 1% Tween20. Molecular weights of protein bands determined by comparing their mobility in gels with those of marker proteins with known molecular masses (PageRuler Prestained Protein Ladder, 10-180 kDa; Thermo Scientific). The antibody dilution used for each antibody was (1: 5,000). The experiment with Trolox was performed in the presence of Trolox (1 mM) to see its effect on protein radical and protein carbonyl formation in thylakoid membranes.

Identification of Oxidatively Modified Residues by Tandem Mass Spectrometry. Oxidatively modified residues of the D1 and D2 proteins were identified by resolving D1 and D2 proteins on a 12.5 to 20% acrylamide lithium dodecyl sulfate-PAGE gradient gel following the methods described in refs. 22, 51, and 52. Following electrophoresis, gels were stained with Coomassie blue, destained, and the D1 and D2 proteins bands were excised. The excised D1 and D2 proteins bands were treated for trypsin digestion using standard protocol. After digestion, the tryptic peptides were processed using a C18 ZipTip before mass analysis and were resolved on a C18 reversed-phase chromatography column. MS was performed on a Thermo Scientific LTQ-FT mass spectrometer following experimental conditions described in Frankel et al. (22). MassMatrix v1.3.2 (53, 54) was used for the identification and analysis of peptides containing oxidative mass modifications and was programmed to search for the presence of oxidative modifications on 19 amino acids, excluding glycine (55, 56). For the identification of oxidative modifications, a $P \leq 1 \times 10^{-5}$ was required, as was a precursor ion mass precision of ≤5.0 ppm. A FASTA library containing the D1, D2, CP47, CP43, PsbO, PsbP, and PsbQ protein sequences and a decoy library containing the same proteins but with reversed amino acid sequences, were investigated. For these experiments, peptides were required to exhibit 0% hits to the decoy library for further consideration.

Molecular Visualization Using PyMol. *PyMol* was used to visualize the D1 and D2 proteins, their oxidatively modified amino acid residues, and their cofactors and ligands, within the cryo-electron microscopy structure of spinach PSII-LHCII super complex (ref. 57, 3.2-Å resolution, PDB ID code 3JCU), and to perform the docking of α-tocopherol in the vicinity of $Pheo_{D1}$, Q_A, and the nonheme iron.

Data Availability. All data needed to evaluate the conclusions in the paper are present in the paper and *SI Appendix*.

ACKNOWLEDGMENTS. This work was funded in part by European Regional Development Fund project "Plants as a tool for sustainable global development" (CZ.02.1.01/0.0/0.0/16_019/0000827) (to A.P. and P.P.); a grant from Palacký University, Olomouc, Czech Republic "Innovative and modern approaches in general and molecular biophysics" IGA_PrF_2020_028 (to A.K.); and US Department of Energy, Office of Basic Energy Sciences Grant DE-FG02-09ER20310 (to T.M.B. and L.K.F.).

1. F. Rappaport, B. A. Diner, Primary photochemistry and energetics leading to the oxidation of the $(Mn)_4Ca$ cluster and to the evolution of molecular oxygen in photosystem II. *Coord. Chem. Rev.* **252**, 259–272 (2008).
2. H. Dau, I. Zaharieva, M. Haumann, Recent developments in research on water oxidation by photosystem II. *Curr. Opin. Chem. Biol.* **16**, 3–10 (2012).
3. D. J. Vinyard, G. W. Brudvig, "Progress toward a molecular mechanism of water oxidation in photosystem II" in *Annual Review of Physical Chemistry*, M. A. Johnson, T. J. Martinez, Eds. (Annual Reviews, Palo Alto, 2017), vol. 68, pp. 101–116.
4. F. J. van Eerden *et al*., Molecular dynamics of photosystem II embedded in the thylakoid membrane. *J. Phys. Chem. B* **121**, 3237–3249 (2017).
5. N. Cox, D. A. Pantazis, W. Lubitz, Current understanding of the mechanism of water oxidation in photosystem II and its relation to XFEL Data. *Annu. Rev. Biochem.* **89**, 795–820 (2020).
6. C. Triantaphylidès, M. Havaux, Singlet oxygen in plants: Production, detoxification and signaling. *Trends Plant Sci.* **14**, 219–228 (2009).
7. P. Pospíšil, Molecular mechanisms of production and scavenging of reactive oxygen species by photosystem II. *Biochim. Biophys. Acta* **1817**, 218–231 (2012).
8. B. B. Fischer, É. Hideg, A. Krieger-Liszkay, Production, detection, and signaling of singlet oxygen in photosynthetic organisms. *Antioxid. Redox Signal.* **18**, 2145–2162 (2013).
9. P. Pospíšil, Production of reactive oxygen species by photosystem II. *Biochim. Biophys. Acta* **1787**, 1151–1160 (2009).
10. R. Kale *et al*., Amino acid oxidation of the D1 and D2 proteins by oxygen radicals during photoinhibition of Photosystem II. *Proc. Natl. Acad. Sci. U.S.A.* **114**, 2988–2993 (2017).
11. P. L. Fine, W. D. Frasch, The oxygen-evolving complex requires chloride to prevent hydrogen peroxide formation. *Biochemistry* **31**, 12204–12210 (1992).
12. A. Arató, N. Bondarava, A. Krieger-Liszkay, Production of reactive oxygen species in chloride- and calcium-depleted photosystem II and their involvement in photoinhibition. *Biochim. Biophys. Acta* **1608**, 171–180 (2004).
13. P. Pospíšil, A. Arató, A. Krieger-Liszkay, A. W. Rutherford, Hydroxyl radical generation by photosystem II. *Biochemistry* **43**, 6783–6792 (2004).
14. D. Takagi, S. Takumi, M. Hashiguchi, T. Sejima, C. Miyake, Superoxide and singlet oxygen produced within the thylakoid membranes both cause photosystem I photoinhibition. *Plant Physiol.* **171**, 1626–1634 (2016).
15. A. Pinnola, R. Bassi, Molecular mechanisms involved in plant photoprotection. *Biochem. Soc. Trans.* **46**, 467–482 (2018).
16. R. Szymanska, I. Slesak, A. Orzechowska, J. Kruk, Physiological and biochemical responses to high light and temperature stress in plants. *Environ. Exp. Bot.* **139**, 165–177 (2017).
17. J. Falk, S. Munné-Bosch, Tocochromanol functions in plants: Antioxidation and beyond. *J. Exp. Bot.* **61**, 1549–1566 (2010).
18. Y. Yamamoto, Quality control of photosystem II. *Plant Cell Physiol.* **42**, 121–128 (2001).
19. L. Lupínková, J. Komenda, Oxidative modifications of the photosystem II D1 protein by reactive oxygen species: From isolated protein to cyanobacterial cells. *Photochem. Photobiol.* **79**, 152–162 (2004).
20. M. Edelman, A. K. Mattoo, D1-protein dynamics in photosystem II: The lingering enigma. *Photosynth. Res.* **98**, 609–620 (2008).
21. A. Kumar, A. Prasad, M. Sedlářová, P. Pospíšil, Characterization of protein radicals in Arabidopsis. *Front. Physiol.* **10**, 958 (2019).
22. L. K. Frankel, L. Sallans, P. A. Limbach, T. M. Bricker, Identification of oxidized amino acid residues in the vicinity of the Mn(4)CaO(5) cluster of photosystem II: Implications for the identification of oxygen channels within the photosystem. *Biochemistry* **51**, 6371–6377 (2012).
23. L. K. Frankel, L. Sallans, P. A. Limbach, T. M. Bricker, Oxidized amino acid residues in the vicinity of $Q_{(A)}$ and $Pheo_{(D1)}$ of the photosystem II reaction center: Putative generation sites of reducing-side reactive oxygen species. *PLoS One* **8**, e58042 (2013).
24. D. A. Weisz, M. L. Gross, H. B. Pakrasi, Reactive oxygen species leave a damage trail that reveals water channels in Photosystem II. *Sci. Adv.* **3**, eaao3013 (2017).
25. J. Sharma *et al*., Primary structure characterization of the photosystem II D1 and D2 subunits. *J. Biol. Chem.* **272**, 33158–33166 (1997).
26. B. M. Greenberg, V. Gaba, A. K. Mattoo, M. Edelman, Identification of a primary in vivo degradation product of the rapidly-turning-over 32 kD protein of photosystem II. *EMBO J.* **6**, 2865–2869 (1987).
27. J. Kruk, H. Holländer-Czytko, W. Oettmeier, A. Trebst, Tocopherol as singlet oxygen scavenger in photosystem II. *J. Plant Physiol.* **162**, 749–757 (2005).
28. M. Price, J. J. Reiners, A. M. Santiago, D. Kessel, Monitoring singlet oxygen and hydroxyl radical formation with fluorescent probes during photodynamic therapy. *Photochem. Photobiol.* **85**, 1177–1181 (2009).
29. P. Pospíšil, Production of reactive oxygen species by photosystem II as a response to light and temperature stress. *Front. Plant Sci.* **7**, 1950 (2016).
30. P. Pospíšil, The role of metals in production and scavenging of reactive oxygen species in photosystem II. *Plant Cell Physiol.* **55**, 1224–1232 (2014).
31. M. J. Davies, Protein oxidation and peroxidation. *Biochem. J.* **473**, 805–825 (2016).
32. A. Bachi, I. Dalle-Donne, A. Scaloni, Redox proteomics: Chemical principles, methodological approaches and biological/biomedical promises. *Chem. Rev.* **113**, 596–698 (2013).
33. A. B. Das *et al*., Rapid reaction of superoxide with insulin-tyrosyl radicals to generate a hydroperoxide with subsequent glutathione addition. *Free Radic. Biol. Med.* **70**, 86–95 (2014).
34. A. Wright, W. A. Bubb, C. L. Hawkins, M. J. Davies, Singlet oxygen-mediated protein oxidation: Evidence for the formation of reactive side chain peroxides on tyrosine residues. *Photochem. Photobiol.* **76**, 35–46 (2002).
35. A. A. Krasnovsky Jr, Singlet molecular oxygen in photobiochemical systems: IR phosphorescence studies. *Membr. Cell Biol.* **12**, 665–690 (1998).
36. D. Marquardt *et al*., Tocopherol activity correlates with its location in a membrane: A new perspective on the antioxidant vitamin E. *J. Am. Chem. Soc.* **135**, 7523–7533 (2013).
37. K. Fukuzawa, W. Ikebata, A. Shibata, T. Sakanaka, S. Urano, "Location of alpha-tocopherol in phospholipid-vesicles and its dynamics in inhibiting lipid-peroxidation" in *Vitamin E: Its Usefulness in Health and in Curing Diseases*, M. Mino, H. Nakamura, A. T. Diplock, H. Kayden, Eds. (Karger, 1993), pp. 31–40.
38. J. Katsaras, R. H. Stinson, J. H. Davis, E. J. Kendall, Location of two antioxidants in oriented model membranes. Small-angle X-ray diffraction study. *Biophys. J.* **59**, 645–653 (1991).
39. G. Vanginkel *et al*., Impact of oxidized lipids and antioxidants, such as vitamin-E and lazaroids, on the structure and dynamics of unsaturated membranes. *J. Chem. Soc. Faraday Trans.* **88**, 1901–1912 (1992).
40. M. Sugiura *et al*., Modification of the pheophytin redox potential in *Thermosynechococcus elongatus* photosystem II with PsbA3 as D1. *Biochim. Biophys. Acta* **1837**, 139–148 (2014).
41. K. Saito, A. W. Rutherford, H. Ishikita, Mechanism of proton-coupled quinone reduction in Photosystem II. *Proc. Natl. Acad. Sci. U.S.A.* **110**, 954–959 (2013).
42. K. Brinkert, S. De Causmaecker, A. Krieger-Liszkay, A. Fantuzzi, A. W. Rutherford, Bicarbonate-induced redox tuning in photosystem II for regulation and protection. *Proc. Natl. Acad. Sci. U.S.A.* **113**, 12144–12149 (2016).
43. S. De Causmaecker, J. S. Douglass, A. Fantuzzi, W. Nitschke, A. W. Rutherford, Energetics of the exchangeable quinone, Q_B, in photosystem II. *Proc. Natl. Acad. Sci. U.S.A.* **116**, 19458–19463 (2019).
44. S. Porfirova, E. Bergmuller, S. Tropf, R. Lemke, P. Dormann, Isolation of an Arabidopsis mutant lacking vitamin E and identification of a cyclase essential for all tocopherol biosynthesis. *Proc. Natl. Acad. Sci. U.S.A.* **99**, 12495–12500 (2002).
45. A. P. Casazza, D. Tarantino, C. Soave, Preparation and functional characterization of thylakoids from *Arabidopsis thaliana*. *Photosynth. Res.* **68**, 175–180 (2001).
46. A. Kumar, A. Prasad, M. Sedlářová, P. Pospíšil, Data on detection of singlet oxygen, hydroxyl radical and organic radical in *Arabidopsis thaliana*. *Data Brief* **21**, 2246–2252 (2018).
47. A. Prasad, M. Sedlářová, A. Balukova, M. Rác, P. Pospíšil, Reactive oxygen species as a response to wounding: In vivo imaging in *Arabidopsis thaliana*. *Front. Plant Sci.* **10**, 1660 (2020).
48. A. Kumar, A. Prasad, M. Sedlářová, P. Pospíšil, Organic radical imaging in plants: Focus on protein radicals. *Free Radic. Biol. Med.* **130**, 568–575 (2019).
49. D. R. Duling, Simulation of multiple isotropic spin-trap EPR spectra. *J. Magn. Reson. B.* **104**, 105–110 (1994).
50. H. Schägger, Tricine-SDS-PAGE. *Nat. Protoc.* **1**, 16–22 (2006).
51. T. Rabilloud, M. Vincon, J. Garin, Micropreparative one- and two-dimensional electrophoresis: Improvement with new photopolymerization systems. *Electrophoresis* **16**, 1414–1422 (1995).
52. G. Sun, V. E. Anderson, Prevention of artifactual protein oxidation generated during sodium dodecyl sulfate-gel electrophoresis. *Electrophoresis* **25**, 959–965 (2004).
53. H. Xu, M. A. Freitas, A mass accuracy sensitive probability based scoring algorithm for database searching of tandem mass spectrometry data. *BMC Bioinformatics* **8**, 133 (2007).
54. H. Xu, M. A. Freitas, MassMatrix: A database search program for rapid characterization of proteins and peptides from tandem mass spectrometry data. *Proteomics* **9**, 1548–1555 (2009).
55. G. Xu, M. R. Chance, Radiolytic modification and reactivity of amino acid residues serving as structural probes for protein footprinting. *Anal. Chem.* **77**, 4549–4555 (2005).
56. J. G. Kiselar, M. R. Chance, Future directions of structural mass spectrometry using hydroxyl radical footprinting. *J. Mass Spectrom.* **45**, 1373–1382 (2010).
57. X. Wei *et al*., Structure of spinach photosystem II-LHCII supercomplex at 3.2 Å resolution. *Nature* **534**, 69–74 (2016).